International Journal of Mass Spectrometry 308 (2011) 71–80

Contents lists available at ScienceDirect

International Journal of Mass Spectrometry

journal homepage: www.elsevier.com/locate/ijms

Structural characterization of cyanidin-3,5-diglucoside and pelargonidin-3,5-diglucoside anthocyanins: Multi-dimensional fragmentation pathways using high performance liquid chromatography-electrospray ionization-ion trap-time of flight mass spectrometry

Jeremy S. Barnes, Kevin A. Schug*

Department of Chemistry and Biochemistry, The University of Texas at Arlington, Arlington, TX, USA

ARTICLE INFO

Article history:
Received 16 May 2011
Received in revised form 26 July 2011
Accepted 26 July 2011
Available online 4 August 2011

Keywords:
Flavonoids
Rose
High mass accuracy
Multi-dimensional fragmentation
Electrospray
LC-ESI-IT-TOF-MS

ABSTRACT

Cyanidin-3,5-diglucoside and pelargonidin-3,5-diglucoside were identified from an extract of freeze-dried red hybrid-tea rose petals with high mass accuracy and multi-dimensional fragmentation using liquid chromatography-electrospray ionization-ion trap-time of flight mass spectrometry (LC-ESI-IT-TOF-MS). The effects of varying the amount of collision energy applied to the trap at each MS stage were studied to optimize subsequent fragmentation steps. Structural characterization of cyanidin and pelargonidin was attempted by identifying the fragments created by cross-ring cleavage (CRC) of the C-ring and small neutral molecule loss. These fragments were further determined to be diagnostic for differentiating the compounds of interest. A computational study of the CRC fragments of cyanidin was performed in order to calculate the overall energy of the fragments. It was determined that the 0,2 CRC pathway was more favorable than the 0,3 CRC pathway.

1. Introduction

Anthocyanins are one of the many compound classes that fall under the polyphenolic flavonoid group; they are plentiful in nature and can be found in leaves, flowers, fruits and vegetables. The core structure of an anthocyanin is a phenolated benzopyran, referred to as a flavylium cation, and may be described as a C_6–C_3–C_6 skeleton. This skeleton has a phenolic ring fused to a pyran with an additional phenolic ring connected at the 2 position of the pyran. Two positions on the B-ring, at 3′ and 5′, provide sites for a variety of substituents and the AC bicycle can be glycosylated at the 3, 5, and 7 positions, which allows for a multitude of potential structural and functional variants. The aglycone flavylium cation is referred to as an anthocyanidin [1] (Fig. 1A). In addition, a positive charge is found on the oxygen of the pyran ring, and provides specific detection from other flavonoid species at 520 nm.

Like many other fruits and flowers, the bright attractive colors of rose petals are partially due to their anthocyanin content. Anthocyanins were investigated in roses as early as 1914 in a study by Willstater and Nolan on the isolation of cyanidin [2]. It was not until 1934 that pelargonidin was identified in a rose [3]. There are six common naturally-occurring anthocyanidins, which are differentiated by hydroxyl and methoxy groups on the B-ring. Each of these aglycones has been detected in one species of flower or another, and are found glycosylated with glucose, rhamnose, fructose, rutinose, and sophorose [4]. One of the most common roses is the red hybrid-tea rose ("Liberty", *R. gallica*). The section *gallicanae* predominately contains cyanidin-3,5-diglucoside, along with small amounts of cyanidin-3-glucoside. Additionally, other anthocyanins, such as pelargonidin-glucosides, can be introduced to these species through genetic recombination [5].

Anthocyanins have been linked to anticancer effects [6], and have demonstrated a capacity to deter apoptosis of cells [7], which may be attributed to their powerful antioxidant abilities [8–11]. Dietary ingestion of these antioxidant compounds is believed to combat oxidative damage by neutralizing reactive radical species. Epidemiological studies have shown that the antioxidant activity provided by the consumption of fruit is positively correlated with reduced mortality from cardiovascular disease and some types of cancer [12]. Recently, attention has been given to anthocyanins and

* Corresponding author at: 700 Planetarium Pl.; Campus box 19065; Arlington, TX 76019-0065, USA. Tel.: +1 817 272 3541; fax: +1 817 272 3808.
E-mail address: kschug@uta.edu (K.A. Schug).

1387-3806/$ – see front matter © 2011 Elsevier B.V. All rights reserved.
doi:10.1016/j.ijms.2011.07.026

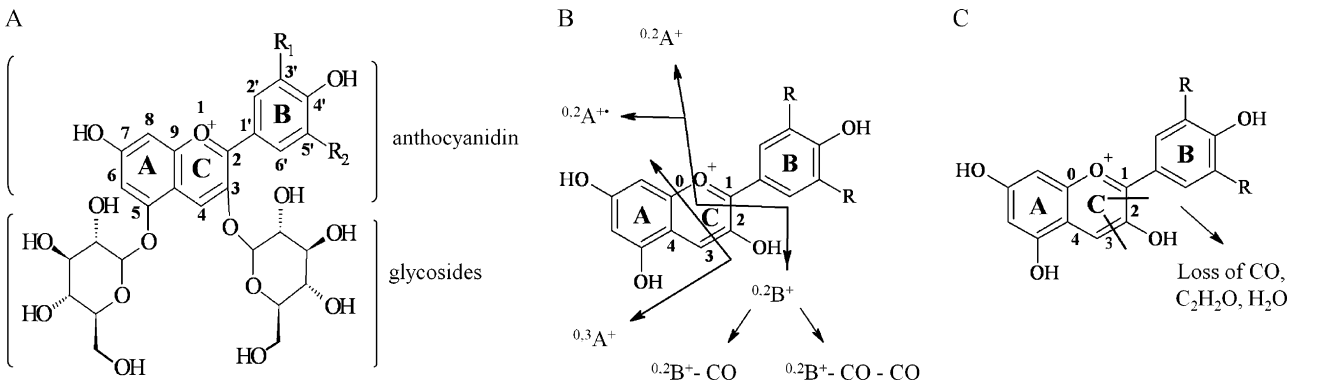

Fig. 1. (A) A generic diglucoside anthocyanin. For pelargonidin, $R_1 = R_2 = H$. For cyanidin, $R_1 = OH$ and $R_2 = H$. Fragmentation of the anthocyanidin generally occurs from either (B) cross-ring cleavage (CRC) or (C) by neutral small molecule loss from ring opening.

their role in signaling pathways related to cancer chemoprevention [13]. Increasing interest in these compounds due to their possible nutritional and therapeutical aspects has led to further need for structural characterization and identification techniques.

Efficient extraction of the compounds from natural material can be accomplished with an acidified aqueous/organic solvent mixture [14]. Analysis is commonly performed using HPLC coupled with UV–vis, photodiode array (PDA), or mass spectrometry (MS) detectors [15]. Often times, the anthocyanin species are isomers of other flavonoids and in complex mixtures, they cannot be differentiated without authentic standards and a separation technique. Additionally, qualitative identification is hindered by the limitation of available commercial standards [16]. Fragmenting the anthocyanidin using collision-induced dissociation (CID) may offer a solution. Positive identification may then be accomplished based on unique diagnostic fragmentation patterns of the anthocyanidin, without the use of commercial standards.

Numerous fragmentation studies have been reported for different flavonoid species, including flavones, isoflavones, flavanones, flavonols and proanthocyanidins [17–24]. Ma et al. demonstrated that the isomeric aglycones from a flavone and a flavonol could be directly identified based on fragmentation patterns of the aglycones [17]. The Brodbelt group used metal complexation to differentiate flavonoid glucuronides [25]. Kang et al. used fragmentation up to MS^5 to discern diagnostic fragmentation patterns for deuterated isoflavones[24]. Another study observed fragmentation up to MS^7 of isoflavones using ESI-IT-TOF-MS [22] and a study of kampferol fragmentation was examined using high mass resolution [23]. Vuckis and Guttman have provided a nice review of structural characterization of flavonoid glycosides by mass spectrometric fragmentation [21].

Anthocyanin fragmentation by low energy CID using a quadrupole ion trap (QIT) is similar to the fragmentation of other flavonoid classes and the products of which can generally be classified into two categories: (1) cross-ring cleavage (CRC) of the C-ring (Fig. 1B); and (2) ring-opening followed by subsequent loss of small neutral molecules, such as CO, C_2H_2O and H_2O (Fig. 1C). Cross-ring cleavage involves the breaking of two bonds of the C-ring. The A-type fragments are the same for most common anthocyanidin species (only very rare species have altered substituents on the A-ring), but the B-type fragments will differ based on the anthocyanidin type, due to changes of the substituents on the B ring [26,27]. These diagnostic B-type fragment ions can aid in confirming the identity of anthocyanins in complex mixtures or in the analysis of unusual plants.

Anthocyanidin fragmentation by a triple quadrupole (QqQ) is believed to be similar to QIT fragmentation, in that, small molecules (CO, H_2O, C_2H_2O) are lost, presumably by single bond cleavage, followed by small molecule ejection, as well as cross-ring cleavage. Studies of anthocyanidin fragmentation by QqQ are limited, and to our knowledge, there currently is no report of observations of A-type cross-ring cleavage fragment ions using a QqQ, although this certainly may be possible. One notable study is from the Montoro group [27], who compared anthocyanidin fragmentation between a QIT and a QqQ. In this study, they observed differences in the fragmentation pattern and intensity profile of the fragment spectra, although many of the small molecule loss ions were observed in both instrument types. Interestingly, they observed a cross-ring cleavage ion at 149 m/z (which would correspond to the $^{0,2}A^+$ ion) using the QIT, which they did not observe in fragment spectra collected using the QqQ.

QIT analysis provides superior qualitative structural analysis, due to its ability to perform iterative fragmentation (MS^n) and high sensitivity, which would be preferred in fragmentation studies. QqQ instruments offer greater quantitative power through MRM, and although fragmentation can be performed, it may be limited to analysis of anthocyanins in natural products due to the stability of the anthocyanidin structure, and since glycoside loss is the dominant fragment mechanism in tandem mass spectrometry of anthocyanins [28,29].

Surprisingly, the literature is incomplete with regard to the mass signals and proposed structures for CRC and small molecule loss fragments for naturally-occurring anthocyanidins. One significant study by Oliveira et al. revealed characteristics of fragmentation patterns for four of the common naturally-occurring anthocyanidins, cyanidin, peonidin, malvidin and delphinidin, using high energy CID by electrospray ionization and orthogonal acceleration-time-of-flight (oa-TOF) tandem mass spectrometry [26]. Other studies involved fragmentation of anthocyanidins from natural product extracts, including berries from a myrtle shrub, grape skins and black carrots, all using ESI and ion trap tandem mass spectrometry [27,30,31]. Literature covering pelargonidin fragmentation is especially limited. A study of black carrots containing pelargonidin glycosides showed fragmentation data but stated that the intensities were too low to obtain reproducible data [31]. Another study attempted fragmentation of pelargonidin following plasma desorption but was not successful [32].

The limited knowledge of anthocyanidin fragmentation may be due to a few associated problems. The flavylium cation is particularly stable and does not easily fragment by low energy CID [26]. Using default instrument settings may leave the user with little or no fragmented species. Second, higher order fragmentation (MS^n) with an ion-trap may be limited because of signal strength, especially with increasing mass stages. During CID in the IT-TOF,

the kinetic energy of the precursor ion is increased through the application of a resonant excitation waveform to the endcaps. The amplitude of this excitation can be varied, and thus, by varying the energy applied to the ion-trap, fragment spectra can be optimized to produce increased signal output. Finally, in low resolution instruments, an observed fragment ion may be assigned as having a large number of possible elemental formulae, particularly with organic compounds, which only contain carbon, hydrogen and oxygen, as in the case of anthocyanins. Increasing the resolution with higher mass accuracy can help eliminate erroneous choices and can provide the user with confidence to propose and assign the exact elemental formula. By applying some heuristic rules, setting the element choices to C, H and O and limiting the mass accuracy to <5 ppm, the number of possible elemental formula for compounds with masses from 100 to 600 Da, can be narrowed to one [33].

Molecular modeling and computational studies of flavonoid compounds may shed some light on the structures of these gas phase fragment ions, which otherwise would be difficult to structurally characterize. There have been a number of different studies focused on computational modeling of anthocyanidins; these have used density functional theory (DFT) [34–36] and *ab initio* [37] approaches. One interesting study showed the effects of varying the hydroxyl substituents on the B-ring of a flavylium cation [38]. Another provided a conformational analysis of pelargonidin using density functional theory [39].

In this study, an electrospray ionization-ion trap-time of flight mass spectrometer equipped with a liquid chromatograph (LC-ESI-IT-TOF-MS) was used to perform higher order fragmentation (up to MS^6) on mono- and diglucosides of cyanidin and pelargonidin found in the petals of a hybrid-tea rose ("Liberty", *R. gallica).* As the collision energy of the ion-trap was adjusted, variations in the signal intensities of product ions were observed, which were due to cleavage of the glycosides at the MS/MS, and MS^3 stages, and then fragmentation of the anthocyanidin at the MS^4 stage and beyond. Iterative fragmentation pathways and high mass accuracy were used to assess the identity of observed mass signals. Software modeling using the density functional theory and the 6–31G basis set was used to help delineate and assign possible CRC mechanisms and product structures.

2. Materials and methods

2.1. Reagents and materials

LCMS-grade acetonitrile, methanol, and water were purchased from Burdick and Jackson (Muskegon, MI, USA). Trifluoroacetic acid (TFA) was purchased from Sigma–Aldrich (St. Louis, MO, USA) and formic acid was purchased from Fluka (AG, Buchs, Switzerland). Red hybrid-tea roses ("Liberty", *R. gallica)* were purchased from a local market.

2.2. Rose petal extraction

Rose petals were ground to a powder in a coffee grinder, and then lyophilized. Powder (0.1 g) was extracted in 70:30:0.1, methanol:water:triflouroacetic acid (1 mL) then centrifuged and filtered to remove any residual solids.

2.3. Instrumentation

Fractionation was performed using a Finnigan SpectraSYSTEM®-HPLC (Thermo-Fisher Scientific, Inc., Waltham, MA, USA) comprised of a P2000 solvent delivery system, an AS3000 autosampler and a UV6000LP diode array detector. A Foxy® Jr. Fraction Collector (Teledyne-Isco, Inc., Lincoln, NE, USA) was placed inline, after the detector. Cyanidin-3,5-diglucoside and pelargonidin-3,5-diglucoside were isolated by eluent collection using the fraction collector. These fractions were further used for ion trap optimization experiments, via direct infusion. Infusion was performed using a NE-1010 syringe pump (New Era Pump Systems Inc. Wantagh, NY, USA) operated at 5 μL/min (Supplemental Figure 1).

Anthocyanin identification and fragmentation was performed on a LCMS-IT-TOF (Shimadzu Scientific Instruments, Kyoto, Japan), equipped with a Prominence HPLC system (LC-20AD pumping system, a SIL-20AHT autosampler, and SPD-M20A diode array detector; Shimadzu). *LCMS Solutions* software (version 3.41.324) was used for data analysis. The *Formula Predictor* function of *LCMS Solutions* was used to support identification, elemental formula generation, and confirmation of unknown signals.

2.4. Ionization parameters and ion-trap optimization

Ionization was performed using a conventional ESI source, in the positive ionization mode. The heat block and curved desolvation line (CDL) were maintained at 250 °C. Nitrogen was used as nebulizing gas and drying gas, each set at 1.5 L/min and 10 L/min, respectively. The ESI source voltage was set to 4.5 kV and the detector voltage was 1.62 V. The ion accumulation time was set at 50 ms. The precursor ion isolation window was set at a width of 3.000 amu and 20 ms. The collision energy CID parameter was varied as demonstrated in the results, while keeping the time and frequency (q) constant at 30 ms and 0.251, respectively. Argon was used as the collision gas, and was set at 50%.

2.5. Chromatographic analysis of extraction

For HPLC-ESI-MS, a Gemini C18 column (100 mm × 2.0 mm, 3 μm; Phenomenex, Torrance, CA, USA) and a Gemini C18 guard column (4.0 × 2.0 mm, 3 μm; Phenomenex) were used to chromatographically separate anthocyanin species using 1.0% formic acid as solvent A and acetonitrile as solvent B. The elution scheme was: linear gradient at 0.1 mL/min from 5% B to 10% B, 0–5 min; isocratic elution 10% B, 5–30 min; linear gradient from 10% B to 13.5% B, 30–75 min; linear gradient from 13.5% B to 25% B, 75–90 min. The eluent was then directed into the ESI source for ionization. The ion trap parameters were set as described in Section 2.4, and the collision energy for CID was set to the optimized energy determined by direct infusion experiments for each mass stage up to MS^4.

2.6. Computational modeling

The 3-D structures of the anthocyanidin fragments and their Cartesian coordinates were submitted to Gaussian 03 [40] for optimization of energy using DFT/B3LYP and 6-31G basis set.

2.7. Nomenclature

The nomenclature described by Ma et al. [17] for labeling fragment ions was used. The labels ${}^{i,j}A^+$ and ${}^{i,j}B^+$ correspond to the fragment ions that contain either the A or B ring and were formed by cleavage of the i and j bonds of the C-ring (Fig. 1B).

3. Results and discussion

3.1. Optimization of glycoside cleavage

The effects of varying the energy applied to the ion-trap on the cleavage of the O-glycosidic bond for the di-glucoside and

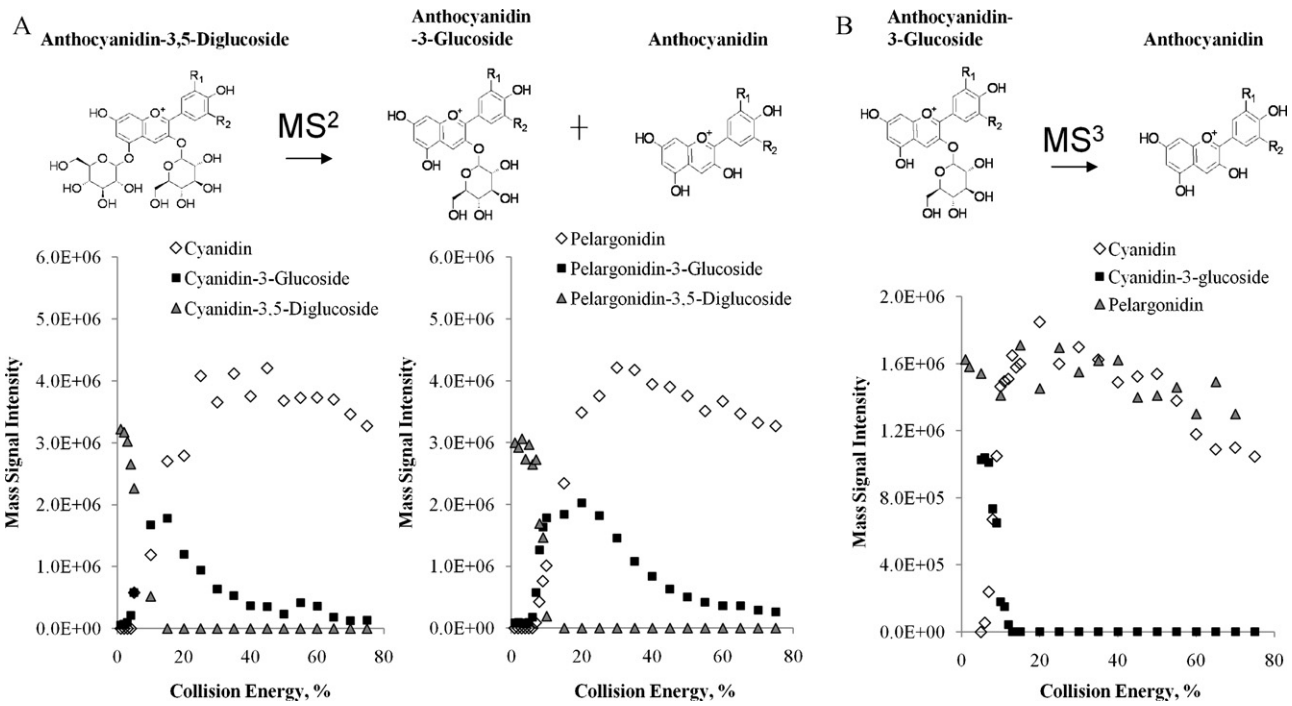

Fig. 2. The effects of varying the collision energy applied to the ion trap on the major fragment ions of cyanidin-3,5-diglucoside and pelargonidin-3,5-diglucoside at (A) MS/MS stage in the positive mode, and (B) at MS^3 stage in the positive mode. For pelargonidin, $R_1 = R_2 = H$. For cyanidin, $R_1 = OH$ and $R_2 = H$.

mono-glucoside species of cyanidin and pelargonidin were observed (Fig. 2A). Both of the anthocyanidin types showed similar trends with regard to loss of their glucose moiety. The loss of the first glucoside from the diglucoside compound was observed at 1% collision energy (the lowest setting). There is some uncertainty as to at which position this glucoside is lost (maybe a mixture of both), but it is depicted in the figures at the 5-position based on the prevalence of the 3-monoglucoside in nature. The mono-glucoside signal grew sharply from 5% to 10%, then reached a maximum and leveled out near 15% for cyanidin and 20% for pelargonidin. From 20% to 75% the signal from the mono-glucoside slowly diminished.

Signals for cyanidin and pelargonidin were observed starting at 5% and 7% collision energy, respectively. At these energies, cleavage of both glucosides was achieved. Operating at collision energies lower than these thresholds could offer the ability to selectively fragment only one glucoside, which might be helpful in distinguishing rare species, which have two different sugar units attached. The anthocyanidin signal quickly supplanted the mono-glucoside signal at 15% collisional energy, suggesting that the energy needed to cleave both glucosides is not that much different than the energy needed for loss of only one glucoside. The anthocyanidin signals reached a maximum near 25% and began to decrease with a mild slope as the collision energy approached 50%, marking the energy at which the anthocyanidin began to fragment. The wide range of consistent signal response from 25% to 75% demonstrates the great stability of the anthocyanidin, while almost all of the collision energy is being directed into cleavage of the glycosides. No fragmentation of the glycoside moieties, besides that of the bond which links it to the anthocyanidin, was observed, typical for product ion spectra of O-glycosides using low energy CID [21]. Additionally, relatively low amounts of protonated signals, $[M+H]^+$, were observed for the diglucoside and mono-glucoside species.

3.2. MS^3: loss of glucoside

Loss of a single glucoside was further studied in the third mass stage by specifically selecting the mono-glucoside and varying the collision energy applied to the trap (Fig. 2B). For cyanidin-monoglucoside, 5% collision energy was not enough to cleave the glucose moiety. At 6%, the aglycone cyanidin ion appeared in the mass spectra and grew sharply until it reached a maximum at 20%. The mono-glucoside signal was absent at this energy, demonstrating that all of the mono-glucoside was fragmented. For pelargonidin-monoglucoside, a different pattern was observed. Already at 1% collision energy, the aglycone signal was near its maximum and the mono-glucoside signal was absent. Two possibilities can be speculated to account for the difference in the amount of minimal collision energy required to observe fragmentation between these species. Either the two ions exhibit different initial internal energies in the trap prior to fragmentation and/or there could be a difference in the stability of the ions based on structure. It seems more likely that there is a real difference in the stability of the structures, since all of the ions are being cooled to a similar extent in the trap, for some time prior to excitation.

3.3. MS^4, MS^5 and MS^6: fragmentation pathways of cyanidin and pelargonidin

It was determined that the maximum amount of signal information from fragmentation of an anthocyanidin could be obtained from within a small window of collision energy values from 10 to 20% maximum collision energy at MS^4 (Fig. 3A). Importantly, the default collision energy setting of 50% collision energy (factory setting on the IT-TOF) would not have provided quality data. The loss of the fragment ion signals at high collision energies may have been due to the destabilization of the parent and product ions along the stability diagram as higher excitation amplitudes were reached. The product ions observed for cyanidin fragmentation (Table 1) are similar to those reported by Montoro et al. [27] and by Downey and Rochfort [30]. They also matched some high energy fragments reported by Oliveira et al. [26], but contrasted significantly in the profile of individual ion intensities. In their study, the CRC fragments were more intense than small molecule loss fragments, while in our spectra, the small molecule loss fragments were

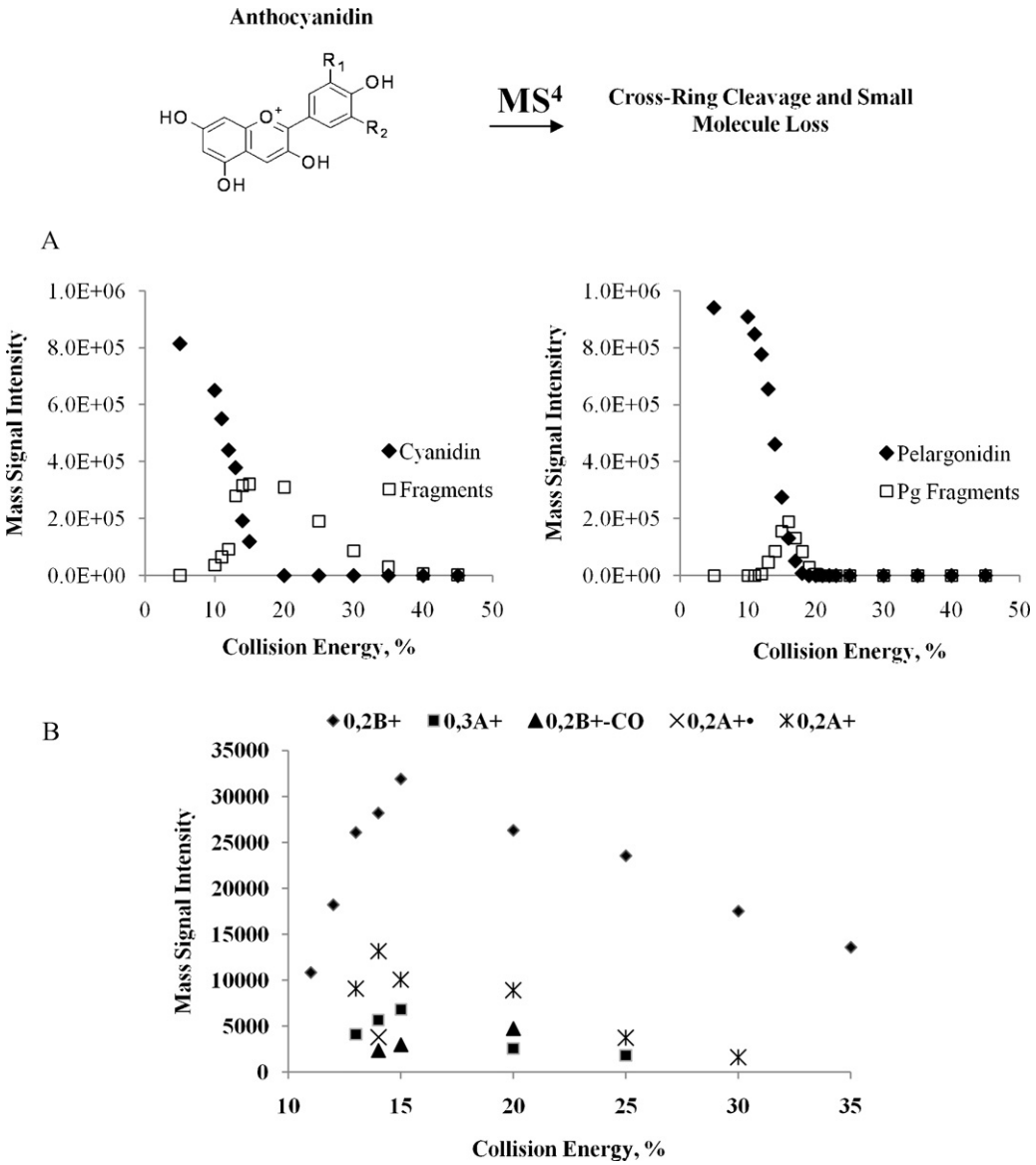

Fig. 3. The effects of varying the collision energy applied to the ion trap at MS^4 stage in the positive mode on (A) the major fragment ions of cyanidin and pelargonidin and (B) the CRC fragment ions of cyanidin. For pelargonidin, $R_1 = R_2 = H$. For cyanidin, $R_1 = OH$ and $R_2 = H$.

more abundant than the CRC fragments (Fig. 4A). The pelargonidin signals (Table 1) also showed some similarities with those reported by Kammerer et al. in a study of black carrots [31]. The profile of the intensities of the product ions showed similar levels of both CRC fragments and small molecule loss (Fig. 4B).

3.4. Cross ring cleavage (CRC)

The cyanidin CRC fragments observed at MS^4 were $^{0,2}A^{+\bullet}$ (150.031 *m*/*z*), $^{0,2}A^{+}$ (149.022 *m*/*z*), $^{0,2}B^{+}$ (137.023 *m*/*z*), $^{0,2}B^{+}$-CO (109.027 *m*/*z*), and $^{0,3}A^{+}$ (121.027 *m*/*z*). Further fragmentation (MS^5) of the $^{0,2}B^{+}$ signal revealed a neutral loss of two carbonyls, giving the signal $^{0,2}B^{+}$-CO–CO (81.034 *m*/*z*), which to our knowledge has not been previously reported. The $^{0,2}A^{+}$ fragment was also observed in fragments of cyanidin, delphinidin, peonidin and malvidin by Montoro et al. [27] using an ion trap mass spectrometer. Based on computational calculations (refer to Sections 3.4.1 and 3.4.2), a structure and mechanism for the generation of the $^{0,2}A^{+}$ was proposed (Fig. 5). This mechanism is similar to the $^{0,2}A^{+\bullet}$ (150.031 *m*/*z*) fragmentation proposed by Oliveira et al. [26], but it involves heterolytic cleavage of bond 2 in the C-ring and a hydrogen transfer from the C-3 hydroxyl group to C-2. Plotting the signal strength of the cyanidin CRC fragments against the collision energy applied to the ion trap showed that the $^{0,2}B^{+}$ fragment is by far the strongest signal, followed by the $^{0,2}A^{+}$, the $^{0,3}A^{+}$ signal, and then, the less intense $^{0,2}A^{+\bullet}$ and $^{0,2}B^{+}$-CO signals (Fig. 3B).

For pelargonidin, a fairly intense signal at 121.028 *m*/*z* was observed in MS^4 spectra, which corresponds to two isobaric CRC fragments, $^{0,3}A^{+}$ and $^{0,2}B^{+}$ (Fig. 4B). Additionally, the $^{0,2}A^{+\bullet}$ (150.029 *m*/*z*), $^{0,2}A^{+}$ (149.023 *m*/*z*), and $^{0,2}B^{+}$-CO (93.031 *m*/*z*) signals were observed. MS^5 fragmentation of the 121.028 *m*/*z* resulted in a neutral loss of a carbonyl, giving $^{0,2}B^{+}$-CO (93.030 *m*/*z*). It is assumed that it was not $^{0,3}A^{+}$-CO because this signal was not observed in the fragmentation of cyanidin and has not been reported previously in the anthocyanidin fragmentation literature.

3.4.1. Computation of the minimized conformation of cross ring cleavage products

A planar cyanidin structure was optimized in Gaussian and portions of the structure were removed to match the CRC fragment

Table 1
The mass signals observed for cyanidin and pelargonidin fragmentation at the MS^4 stage in the positive mode, and their proposed neutral losses based on mass accuracy and predicted elemental formula.

Fragment type	Cyanidin			Pelargonidin		
	Theoretical mass, *m/z*	Measured Signal, *m/z*	Error (ppm)	Theoretical mass, *m/z*	Measured Signal, *m/z*	Error (ppm)
3,5-Diglucoside	611.1607	611.1610	0.6	595.1657	595.1648	−1.6
3-Diglucoside	449.1078	449.1088	2.1	433.1129	433.1114	−3.5
Anthocyanidin	287.0550	287.0548	−0.7	271.0601	271.0594	−2.6
$^{0,2}A^+$	149.0233	149.0219	−9.4	149.0233	149.0225	−5.4
$^{0,2}A^{+\bullet}$	150.0311	150.0309	−1.6	150.0311	150.0287	−16.3
$^{0,3}A^+$	121.0284	121.0273	−9.1	121.0284	121.0279	−4.2
$^{0,2}B^+$	137.0233	137.0226	−5.3	121.0284	121.0279	−4.2
$^{0,2}B^+$-CO	109.0284	109.0268	−14.7	93.0302	93.0313	11.8
$^{0,2}B^+$-CO–CO	81.0335	81.0337	2.6	65.03858	N/A	N/A
M−H_2O	269.0444	269.0424	−7.6	253.0495	253.0501	2.2
M−CO	259.0601	259.0624	8.9	243.0652	243.0640	−4.9
M−H_2O–CO	241.0495	241.0494	−0.6	225.0546	225.0538	−3.7
M−CO–CO	231.0652	231.0641	−4.7	215.0703	215.0719	7.6
M−H_2O–C_2H_2O	227.0339	227.0356	7.6	211.0407	N/A	N/A
M−H_2O–CO–CO	213.0546	213.0560	6.5	197.0597	197.0599	1.0
M−CO–CO–CO	203.0703	203.0704	0.6	187.0754	187.0739	−7.8
M−H_2O–CO–C_2H_2O	199.0390	199.0405	7.7	183.0441	183.0451	5.7
M−H_2O–CO–CO–H_2O	195.0441	195.0450	4.8	179.0491	N/A	N/A
M−CO–CO–C_2H_2O	189.0546	189.0546	−0.1	173.0597	173.0579	−10.4
M−H_2O–CO–CO–CO	185.0597	185.0596	−0.6	169.0648	169.0650	1.2
M−CO–CO–CO–CO	175.0754	N/A	N/A	159.0804	159.0789	−9.7
M−C_2H_2O–C_2H_2O–CO	175.0390	175.0393	1.9	159.0441	159.0454	8.4
M−H_2O–CO–CO–C_2H_2O	171.0441	171.0435	−3.2	155.0491	155.0490	−0.9
M−H_2O–CO–CO–CO–H_2O	167.0491	167.0510	11.1	151.0542	151.0512	−20.1
M−CO–CO–C_5H_6	165.0182	165.0160	−13.5	149.0233	N/A	N/A
M−CO–CO–C_4H_2O	163.0390	163.0398	5.1	147.0441	N/A	N/A
M−CO–CO–C_2H_2O–CO	161.0597	161.0585	−7.5	145.0648	145.0653	3.5
M−C_2H_2O–C_2H_2O–CO–O + H	160.0519	160.0537	11.4	144.0570	N/A	N/A
M−H_2O–CO–CO–CO–CO	157.0648	157.0657	5.8	141.0699	141.0693	−4.1
M−C_2H_2O–C_2H_2O–CO–CO	147.0441	147.0428	−8.5	131.0491	N/A	N/A
M−H_2O–CO–CO–C_2H_2O–CO	143.0491	143.0511	13.7	127.0542	127.0528	−11.3
M−H_2O–CO–CO–H_2O–CO–CO + H_2	141.0699	141.0702	2.3	125.0750	N/A	N/A
M−H_2O–CO–CO–H_2O–CO–CO	139.0542	139.0534	−6.0	123.0593	N/A	N/A
M−CO–CO–C_2H_2O–CO–CO	133.0708	N/A	N/A	117.0759	117.0781	18.6
M−CO–CO–C_2H_2O–CO–CH_2O	131.0491	N/A	N/A	115.0542	115.0541	−1.1
M−H_2O–CO–CO–CO–CO–CO	129.0699	129.0714	11.8	113.0750	N/A	N/A
M−H_2O–CO–CO–CO–CO–CO–H	128.0621	128.0613	−5.9	112.0671	N/A	N/A
M−H_2O–CO–CO–CO–CO–CO–H_2	127.0542	127.0552	7.7	111.0593	N/A	N/A
M−C_2H_2O–C_2H_2O–CO–CO–CO	119.0491	119.0469	−18.8	103.0542	N/A	N/A
M−H_2O–CO–CO–C_2H_2O–CO–CO	115.0542	115.0546	3.2	99.0593	N/A	N/A

N/A = Not available; a corresponding signal was not observed.

types. The lowest energy conformation of the fragment was then computed. The optimized structures were compared to the structures proposed by Oliveira et al. [26] and Montoro et al. [27]. The $^{0,2}A^+$ structure proposed herein differs from the one proposed by Montoro et al. [27]. Their structure suggests that a hydrogen is transferred from the C-4 to C-9, leaving a formal charge on the C-4, and a straight C–C–O chain. As seen in Fig. 6, many of the computed structures matched their proposed counterparts, which provides some justification of their existence in the gas phase, including the structure for $^{0,2}A^+$, which we proposed.

3.4.2. Correlation of energy values vs. observed fragmentation of cross-ring cleavage products

In the CRC fragmentation scheme, the precursor ion fragments to form both charged and neutral species. Software-calculated energy values for each charged and neutral fragment of cyanidin were obtained and compared against each other (Supplemental Tables 1 and 2). The combined computed lowest energy values of fragments were in good agreement with the computed lowest energy of the non-fragmented species. From estimating the change in energy relative to the charged cyanidin parent ion, it can be determined that the $^{0,2}A^+$ and $^{0,2}B^+$ fragments are the most energetically favorable products. Additionally, it can be implied that the $^{0,2}A/B^+$ fragment scheme is more energetically favorable than the $^{0,3}A/B^+$ fragment scheme.

The computational values for the $^{0,2}A/B^+$ scheme are in agreement with the intensities of the CRC fragments observed experimentally (Fig. 3B). Based on the change in energy relative to cyanidin, the $^{0,2}A^+$ fragment is the most energetically favorable ion to be formed compared to the other CRC fragments, but the observed intensities for this fragment are lower than the $^{0,2}B^+$ ions. The transfer of hydrogen needed to generate the $^{0,2}A^+$ fragment may create a higher activation barrier leading to lower fragment intensities. The $^{0,2}A^{+\bullet}$ fragment ions were very low in intensity, which is in contrast to what is suggested by the computational values. The reason for this may be due to the highly reactive and short-lived nature of the radical in the ion trap.

A possible rearrangement of the $^{0,3}A^+$ ion into a tropylium configuration was also evaluated based on the energy determined by computational calculations. The calculated energy for the tropylium-style ion structure was higher in energy than the structure initially proposed by Oliveira et al. [26] (Supplemental Table 1). Additionally, when allowed to reconfigure after removing the appropriate atoms from the anthocyanidin, to simulate a cross-ring cleavage (as in the natural conformation simulation above), the structure formed was identical to the structure proposed by Oliveira et al. [26]. Still, a possibility exists that there could be

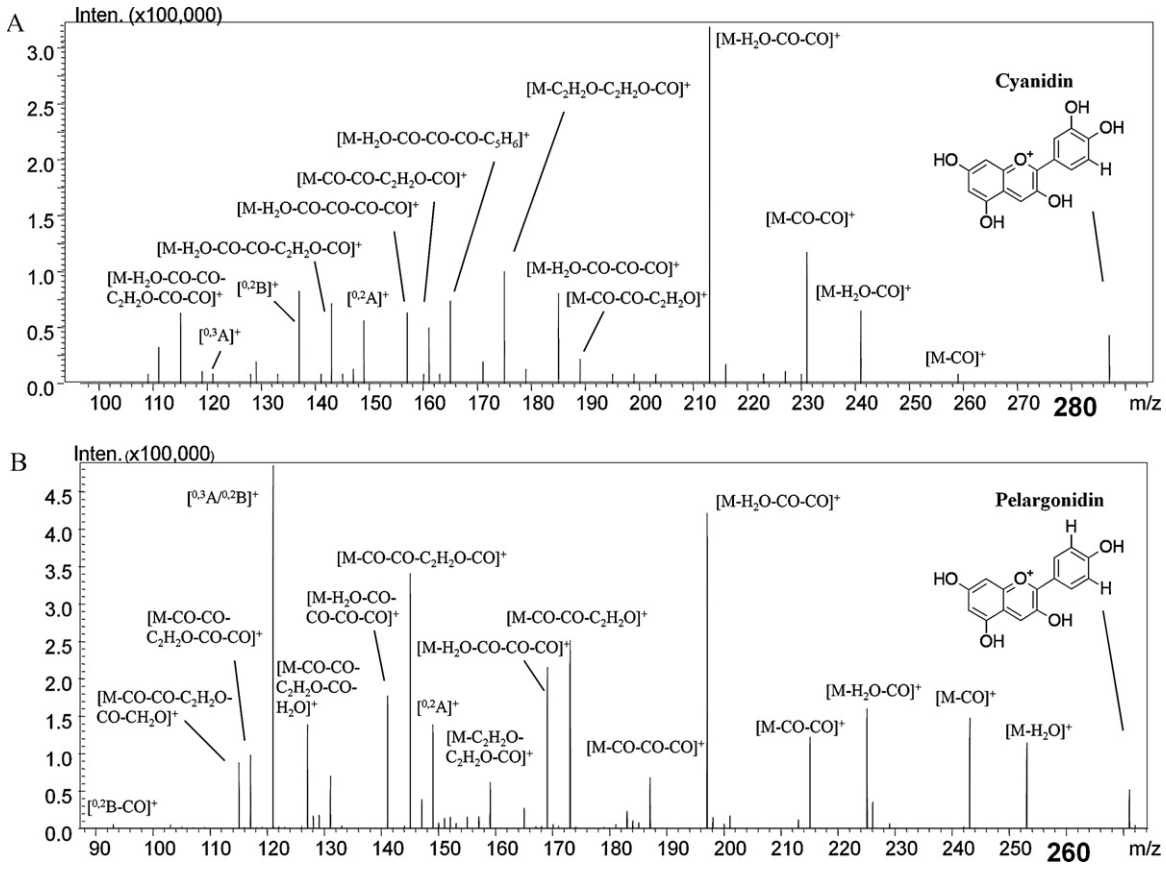

Fig. 4. The product ion spectra of (A) cyanidin and (B) pelargonidin at MS^4 stage in the positive mode.

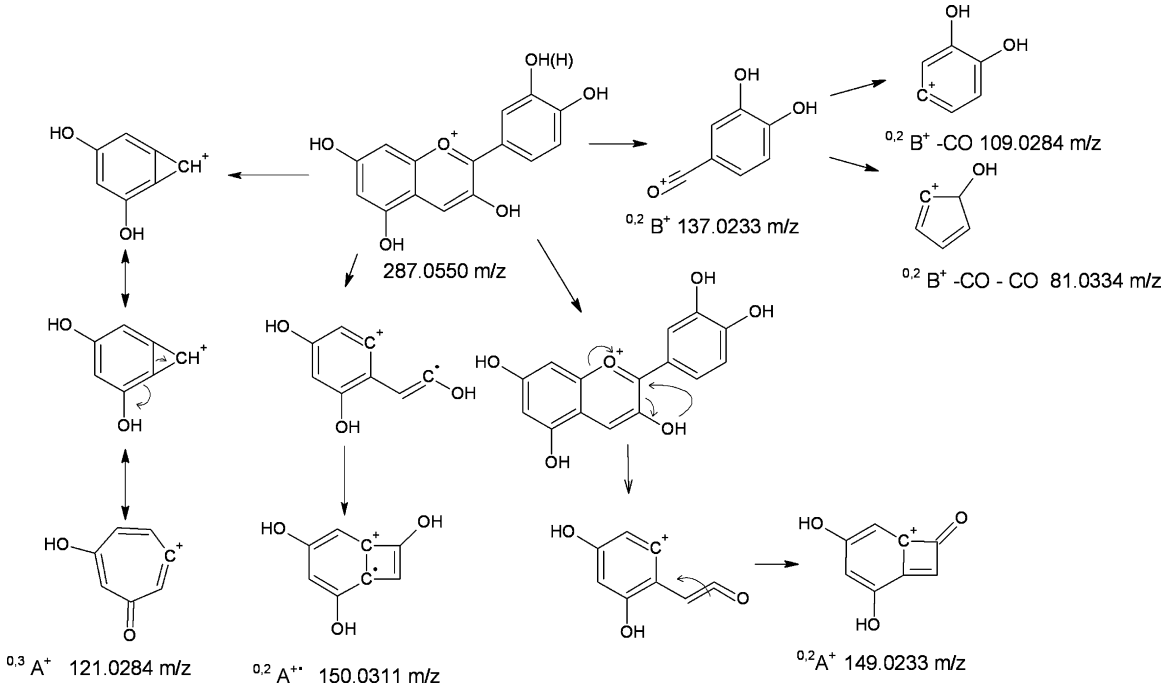

Fig. 5. Proposed structures and mechanisms for CRC fragmentation of cyanidin.

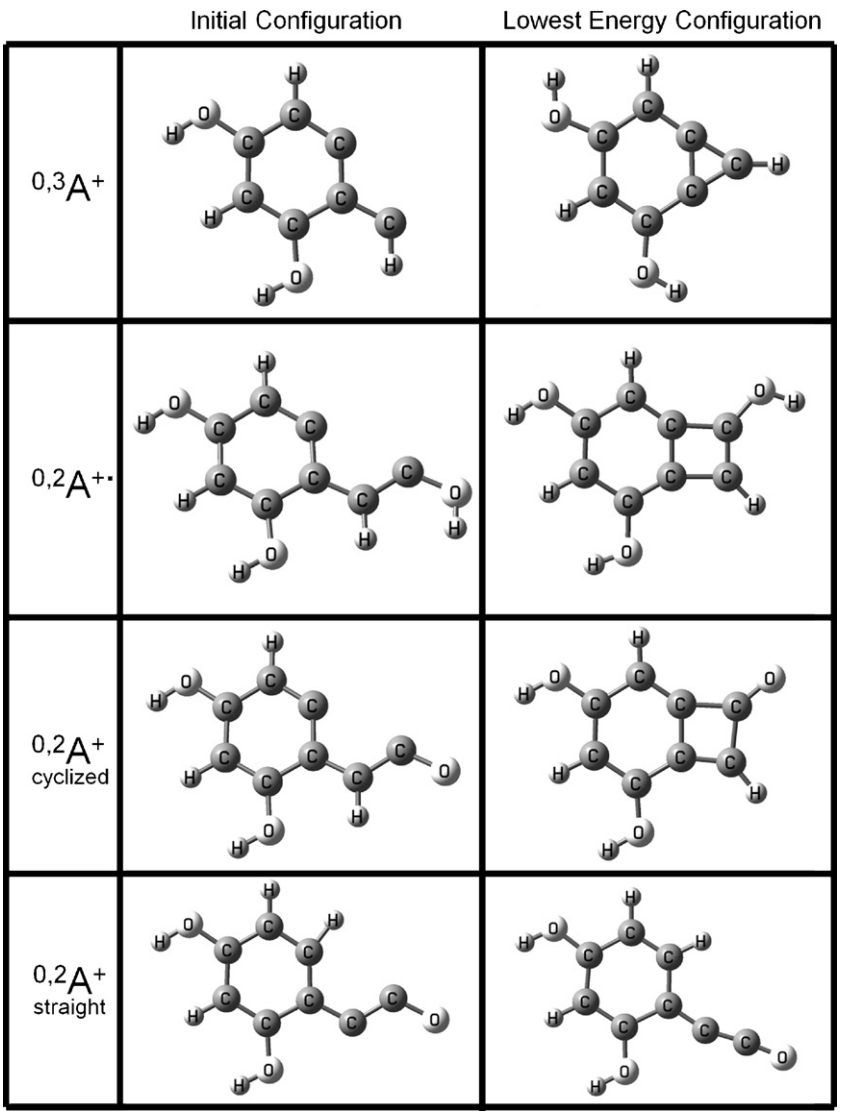

Fig. 6. Minimized conformations of cross-ring cleavage structures by computational analysis using DFT/B3LYP and 6-31G basis set.

a more energetically favorable intermediate, which would favor formation of the tropylium ion.

3.5. Ring opening and small molecule loss

Due to the high stability of the anthocyanidin structure, there can be some speculation as to which ring is opening to facilitate fragmentation by small molecule loss. Based on the CRC fragmentation pattern, it can be assumed that a cleavage site can be found at bonds 2 or 3 of the C-ring (Fig. 1C). Loss of CO from the C-3 position would then be justifiable. This fragmentation could also lead to a number of other possible fragmentation scenarios.

There are an enormous number of possible fragmentation schemes, and due to isobaric uncertainties, the structures related to each of these fragmentation events may not be easily distinguished based on mass signals alone, or readily proven since some of these species may only exist for a short amount of time within the confines of the instrument. Some diagnostic information can be assessed, though, by comparing the type of fragmentation observed for each anthocyanidin species.

In addition to multi-stage fragmentation, high mass accuracy was used in assigning the neutral losses of fragment ions. For example, the loss of CO (27.996 Da) can be differentiated from the loss of C_2H_4 (28.031 Da) by determining the accuracy between the observed signal and the theoretical monoisotopic mass. The difference between the theoretical masses of $[M-CO]^+$ (259.060 m/z) and $[M-C_2H_4]^+$ (259.024 m/z) is ~140 ppm. Another example can be illustrated by two observed signals in the pelargonidin fragmentation: 159.079 m/z and 159.045 m/z. These fragment signals were assigned as $[M-CO-CO-CO-CO]^+$ (theor. 159.080 m/z, −9.7 ppm error) and $[M-C_2H_2O-C_2H_2O-CO]^+$ (theor. 159.044 m/z, 8.4 ppm error), respectively. Although the instrument is calibrated to <5 ppm mass accuracy, at higher stages, ion intensity can be greatly reduced and thus the mass accuracy can be affected due to the low ion intensity. In general, assignments were only considered justifiable when the error was within 25 ppm mass accuracy, a conservative value based on the IT-TOF mass spectrometer performance.

3.5.1. Cyanidin fragmentation

In the case of the cyanidin species, the neutral small molecules lost were all either water (H_2O), carbonyl (CO), C_5H_6 and/or ketene (C_2H_2O). Based on which small molecule was lost, a specific fragmentation pathway was observed. In our experience, fragmentation may continue to occur until there is no more oxygen left in the fragment species, granted the precursor sig-

nal is of suitable strength and the appropriate collision energy is applied. For example, during the fragmentation of cyanidin-3,5-diglucoside, a fragment ion at 128.062 m/z was observed in the MS^6 stage. Based on the iterative fragment pathway and mass accuracy, −5.9 ppm error, the signal is assumed to be [cyanidin–H_2O–CO–CO–CO–CO–CO–H]$^{+\cdot}$, which corresponds to a loss of 6 oxygens, the number of oxygens cyanidin contains (Table 1 and Supplemental Table 3). Similarly, during the fragmentation of pelargonidin-3,5-diglucoside, a fragment ion at 141.069 m/z was observed in the MS^6 stage. Based on the iterative fragmentation pathway and mass accuracy, −4.1 ppm error, the signal is assumed to be [pelargonidin–H_2O–CO–CO–CO–CO]$^+$, which is the loss of 5 oxygens, the number of oxygens pelargonidin contains (Table 1 and Supplemental Table 4). For this reason, the fragment types that include a loss of 6 oxygens (by way of CO/H_2O/C_2H_2O loss) were only observed for cyanidin fragmentation, and not for fragmentation of pelargonidin.

Signals for loss of water, [M−H_2O]$^+$ (269.042 m/z) and loss of a carbonyl [M−CO]$^+$ (259.062 m/z) were observed in the MS^4 spectrum. Iterative fragmentation of [M−H_2O]$^+$ at MS^5 resulted in further losses of CO and C_2H_2O (Supplemental Table 3). Further fragmentation of the signals [M−CO]$^+$ could not be collected either due to an insufficient signal level or improper collision energy applied, although, fragmentation of [M−CO–CO]$^+$ was easily obtained.

The fragment at 175.039 m/z is believed to be [M−C_2H_2O–C_2H_2O–CO]$^+$. This fragment is believed to be a primary fragment since it was not observed in the H_2O or CO pathways and because neither [M−C_2H_2O]$^+$ nor [M−C_2H_2O–C_2H_2O]$^+$ were observed.

There are two routes by which the fragment ion at 213.056 m/z could be formed, based on the fact that it was observed from two separate parent fragments, [M−H_2O–CO]$^+$ (241.049 m/z) and [M−CO–CO]$^+$ (231.064 m/z) (Supplemental Table 3). This makes the proposal of structures for the fragments from 213.056 m/z difficult, because fragments may have been generated from two separate species which had the same mass. A combined response of two isobaric fragment ions would help explain why this signal was the most intense in the MS^4 spectrum (Fig. 4B).

3.5.2. *Pelargonidin fragmentation*

Fragmentation of pelargonidin at MS^4 also demonstrated loss of small neutral molecules, CO, H_2O, and C_2H_2O, in a manner similar to cyanidin. Pelargonidin differed from cyanidin in losses of CH_2O and C_5H_2O groups. Also, it is worth noting that further fragmentation of the ions assigned as [M−CO]$^+$ was successful (Supplemental Table 3), unlike for cyanidin. However, this may only have been due to sufficient signal level or adequate collision energy applied.

Unexpectedly, all of the pelargonidin fragments signals were different from the cyanidin signals by at least one mass unit, except the masses 141.069 m/z and 115.054 m/z, even though the two compounds share many of the same type of fragmentation signals (Table 1). Signals with the same mass would be expected in both fragmentation spectra if a substantial amount of the B-ring was cleaved. This suggests that ring opening and small molecule loss may be primarily originating in the A–C bicycle since the B-ring substituents would provide the 16 unit mass difference observed between the majority of the common fragment signal types shared between the two anthocyanidins.

Finally, the substituents of the B-ring may be directing certain fragmentation pathways. This would lead to unique fragment ions that were only observed in fragment spectra of certain anthocyanidin species. For example, [M−H_2O–C_2H_2O]$^+$ was observed in the cyanidin spectra, but not in the pelargonidin spectra. This fragment pathway may be preferred due to the fact that cyanidin has two hydroxyl groups in the B-ring which could both be lost in consecutive fragmentation events. Pelargonidin would not be able to follow this pathway, since it has only one hydroxyl group.

4. Conclusion

Fragmentation of cyanidin-3,5-diglucoside and pelargonidin-3,5-diglucoside was shown to be greatly affected by the amount of energy applied to the ion trap. Optimization of this energy was shown to increase the signal strength of various product ions, which improved the ability to achieve higher order fragmentation. Fragmentation of cyanidin and pelargonidin was found to occur within a narrow range of collision energies to give cross-ring cleavage and small neutral molecule loss products.

The cross ring cleavage fragments of cyanidin generated by breaking the C_9–O_1 and C_2–C_3 bonds (0,2 pathway) were found to be in greater intensity than the fragments generated from cleaving the C_9–O_1 and C_3–C_4 bonds (0,3 pathway) and this trend was further justified by computational calculations.

Ring opening fragments of cyanidin and pelargonidin were found to lose CO, H_2O and C_2H_2O, while pelargonidin also showed losses of CH_2O and C_5H_2O. Additionally, all of the CRC product ions from the CID of each anthocyanidin, except for two, were shown to be diagnostic in differentiating cyanidin and pelargonidin.

Overall, clear differences in the higher order fragmentation of these anthocyanin species indicates that such information could eventually be used for unequivocal identification of these important compounds in natural product extracts, especially when combined with high efficiency separations.

Acknowledgements

The authors gratefully acknowledge support for instrumentation from the Shimadzu Equipment Grants for Research Program.

Appendix A. Supplementary data

Supplementary data associated with this article can be found, in the online version, at doi:10.1016/j.ijms.2011.07.026.

References

[1] J.B. Harborne, The Flavonoids: Advances in Research Since 1986, Chapman and Hall, University Press, Cambridge, Great Britain, 1994.
[2] R. Willstatter, T.J. Nolan, The pigment of the rose, Anal. Chem. 408 (1914) 1–14.
[3] G.M. Robinson, R. Robinson, A Survey of anthocyanins. II, Biochem. J. 26 (1932) 1647–1664.
[4] Y. Mikanagi, N. Saito, M. Yokoi, F. Tatsuzawa, Anthocyanins in flowers of genus *Rosa*, sections *Cinnamomeae* (=*Rosa*), *Chinenses* Gallicanae and some modern garden roses, Biochem. Syst. Ecol. 28 (2000) 887–902.
[5] C.H. Eugster, E. Märki-Fischer, The chemistry of rose pigments, Angew. Chem. Int. Ed. Engl. 30 (1991) 654–672.
[6] I. Fernandes, A. Faria, J. Azevedo, S. Soares, C. Calhau, V. De Freitas, N. Mateus, Influence of anthocyanins, derivative pigments and other catechol and pyrogallol-type phenolics on breast cancer cell proliferation, J. Agric. Food Chem. 58 (2010) 3785–3792.
[7] H.B. Park, Y.-S. Hah, J.-W. Yang, J.-B. Nam, S.-H. Cho, S.-T. Jeong, Antiapoptotic effects of anthocyanins on rotator cuff tenofibroblasts, J. Orthop. Res. 28 (2010) 1162–1169.
[8] J.A. Vinson, L. Zubik, P. Bose, N. Samman, J. Proch, Dried fruits: excellent *in vitro* and *in vivo* antioxidants, J. Am. Coll. Nutr. 24 (2005) 44–50.
[9] R.A. Moyer, K.E. Hummer, C.E. Finn, B. Frei, R.E. Wrolstad, Anthocyanins, phenolics, and antioxidant capacity in diverse small fruits: vaccinium, rubus, and ribes, J. Agric. Food Chem. 50 (2002) 519–525.
[10] C. Rice-Evans, N. Miller, G. Paganga, Antioxidant properties of phenolic compounds, Trends Plant Sci. 2 (1997) 152–159.
[11] D. Huang, B. Ou, R.L. Prior, The chemistry behind antioxidant capacity assays, J. Agric. Food Chem. 53 (2005) 1841–1856.
[12] A. Faria, J. Oliveira, P. Neves, P. Gameiro, C. Santos-Buelga, V. de Freitas, N. Mateus, Antioxidant properties of prepared blueberry (*Vaccinium myrtillus*) extracts, J. Agric. Food Chem. 53 (2005) 6896–6902.
[13] D.X. Hou, Potential mechanisms of cancer chemoprevention by anthocyanins, Curr. Mol. Med. 3 (2003) 149–159.

[14] J.S. Barnes, H.P. Nguyen, S. Shen, K.A. Schug, General method for extraction of blueberry anthocyanins and identification using high performance liquid chromatography-electrospray ionization-ion trap-time of flight-mass spectrometry, J. Chromatogr. A 1216 (2009) 4728–4735.
[15] Z. Zhang, X. Kou, K. Fugal, J. McLaughlin, Comparison of HPLC methods for determination of anthocyanins and anthocyanidins in bilberry extracts, J. Agric. Food Chem. 52 (2004) 688–691.
[16] J.M. Harnly, R.F. Doherty, G.R. Beecher, J.M. Holden, D.B. Haytowitz, S. Bhagwat, S. Gebhardt, Flavonoid content of U.S. fruits, vegetables, and nuts, J. Agric. Food Chem. 54 (2006) 9966–9977.
[17] Y.L. Ma, Q.M. Li, H. Van den Heuvel, M. Claeys, Characterization of flavones and flavonol aglycones by collision-induced dissociation tandem mass spectrometry, Rapid Commun. Mass Spectrom. 11 (1997) 1357–1364.
[18] N. Fabre, I. Rustan, E. de Hoffmann, J. Quetin-Leclercq, Determination of flavone, flavonol and flavanones aglycones by negative ion liquid chromatography-electrospray ion trap mass spectrometry, J. Am. Soc. Mass Spectrom. 12 (2001) 707–715.
[19] D. Callemien, S. Collin, Use of RP-HPLC-ESI(−)-MS/MS to differentiate various proanthocyanidin isomers in lager beer extracts, J. Am. Soc. Brew. Chem. 66 (2008) 109–115.
[20] H.-J. Li, M.L. Deinzer, Tandem mass spectrometry for sequencing proanthocyanidins, Anal. Chem. 79 (2007) 1739–1748.
[21] V. Vukics, A. Guttman, Structural characterization of flavonoid glycosides by multi-stage mass spectrometry, Mass Spectrom. Rev. 29 (2010) 1–16.
[22] H. Li, L. Wan, Y. Hashi, S. Chen, Fragmentation study of a 8-C-glycosyl isoflavone, puerarin, using electrospray ion trap time-of-flight mass spectrometry at high resolution, Rapid Commun. Mass Spectrom. 21 (2007) 2497–2504.
[23] R.E. March, X.-S. Miao, A fragmentation study of kaempferol using electrospray quadrupole time-of-flight mass spectrometry at high mass resolution, Int. J. Mass Spectrom. 231 (2004) 157–167.
[24] J. Kang, L.A. Hick, W.E. Price, A fragmentation study of isoflavones in negative electrospray ionization by MS^n ion trap mass spectrometry and triple quadrupole mass spectrometry, Rapid Commun. Mass Spectrom. 21 (2007) 857–868.
[25] B.D. Davis, P.W. Needs, P.A. Kroon, J.S. Brodbelt, Identification of isomeric flavonoid glucuronides in urine and plasma by metal complexation and LC-ESI-MS/MS, J. Mass Spectrom. 41 (2006) 911–920.
[26] M.C. Oliveira, P. Esperanca, M.A. Almoster Ferreira, Characterisation of anthocyanidins by electrospray ionization and collision-induced dissociation tandem mass spectrometry, Rapid Commun. Mass Spectrom. 15 (2001) 1525–1532.
[27] P. Montoro, C.I.G. Tuberoso, A. Perrone, S. Piacente, P. Cabras, C. Pizza, Characterisation by liquid chromatography-electrospray tandem mass spectrometry of anthocyanins in extracts of *Myrtus communis* L. berries used for the preparation of myrtle liqueur, J. Chromatogr. A 1112 (2006) 232–240.
[28] Q. Tian, M.M. Giusti, G.D. Stoner, S.J. Schwart, Screening for anthocyanins using high-performance liquid chromatography coupled to electrospray ionization tandem mass spectrometry with precursor-ion analysis, product-ion analysis, common-neutral-loss analysis, and selected reaction monitoring, J. Chromatogr. A. 1091 (2005) 72–82.
[29] J. Valls, S. Millan, M.P. Martí, E. Borras, L. Arola, Advanced separation methods of food anthocyanins, isoflavones and flavanols, J. Chromatogr. A 1216 (2009) 7143–7172.
[30] M.O. Downey, S. Rochfort, Simultaneous separation by reversed-phase high-performance liquid chromatography and mass spectral identification of anthocyanins and flavonols in Shiraz grape skin, J. Chromatogr. A 1201 (2008) 43–47.
[31] D. Kammerer, R. Carle, A. Schieber, Detection of peonidin and pelargonidin glycosides in black carrots (*Daucus carota* ssp Sativus var. atrorubens Alef.) by high-performance liquid chromatography/electrospray ionization mass spectrometry, Rapid Commun. Mass Spectrom. 17 (2003) 2407–2412.
[32] K.V. Wood, C.C. Bonham, J. Ng, J. Hipskind, R. Nicholson, Plasma desorption mass spectrometry of anthocyanidins, Rapid Commun. Mass Spectrom. 7 (1993) 400–403.
[33] T. Kind, O. Fiehn, Seven golden rules for heuristic filtering of molecular formulas obtained by accurate mass spectrometry, BMC Bioniformatics 8 (105) (2007) 1–20.
[34] R. Guzman, C. Santiago, M. Sanchez, A density functional study of antioxidant, properties, on anthocyanins, J. Mol. Struct. 935 (2009) 110–114.
[35] J.N. Woodford, A DFT investigation of anthocyanins, Chem. Phys. Lett. 410 (2005) 182–187.
[36] M. Wolniak, I. Wawer, ^{13}C CPMAS NMR and DFT calculation of anthocyanidins, Solid State Nucl. Magn. Reson. 34 (2008) 44–51.
[37] K. Sakata, N. Saito, T. Honda, Ab initio study of molecular structures and excited states in anthocyanidins, Tetrahedron 62 (2006) 3721–3731.
[38] G.K. Pereira, P.M. Donate, S.E. Galembeck, Effects of substitution for hydroxyl in the B-ring of the flavylium cation, Theochem. J. Mol. Struct. 392 (1997) 169–179.
[39] L. Estevez, R.A. Mosquero, A density functional theory study on pelargonidin, J. Phys. Chem. A 111 (2007) 11100–11109.
[40] Gaussian 03, Revision C.02, M.J. Frisch, G.W. Trucks, H.B. Schlegel, G.E. Scuseria, M.A. Robb, J.R. Cheeseman, J.A. Montgomery, Jr., T. Vreven, K.N. Kudin, J.C. Burant, J.M. Millam, S.S. Iyengar, J. Tomasi, V. Barone, B. Mennucci, M. Cossi, G. Scalmani, N. Rega, G.A. Petersson, H. Nakatsuji, M. Hada, M. Ehara, K. Toyota, R. Fukuda, J. Hasegawa, M. Ishida, T. Nakajima, Y. Honda, O. Kitao, H. Nakai, M. Klene, X. Li, J.E. Knox, H.P. Hratchian, J.B. Cross, V. Bakken, C. Adamo, J. Jaramillo, R. Gomperts, R.E. Stratmann, O. Yazyev, A.J. Austin, R. Cammi, C. Pomelli, J.W. Ochterski, P.Y. Ayala, K. Morokuma, G.A. Voth, P. Salvador, J.J. Dannenberg, V.G. Zakrzewski, S. Dapprich, A.D. Daniels, M.C. Strain, O. Farkas, D.K. Malick, A.D. Rabuck, K. Raghavachari, J.B. Foresman, J.V. Ortiz, Q. Cui, A.G. Baboul, S. Clifford, J. Cioslowski, B.B. Stefanov, G. Liu, A. Liashenko, P. Piskorz, I. Komaromi, R.L. Martin, D.J. Fox, T. Keith, M.A. Al-Laham, C.Y. Peng, A. Nanayakkara, M. Challacombe, P.M.W. Gill, B. Johnson, W. Chen, M.W. Wong, C. Gonzalez, J.A. Pople, Gaussian, Inc., Wallingford CT, 2004.